NANO LETTERS

Letter

pubs.acs.org/NanoLett

Correlating Electronic Transport to Atomic Structures in Self-Assembled Quantum Wires

Shengyong Qin,[†] Tae-Hwan Kim,[†] Yanning Zhang,[‡] Wenjie Ouyang,[‡] Hanno H. Weitering,[§] Chih-Kang Shih,[∥] Arthur P. Baddorf,[†] Ruqian Wu,[‡] and An-Ping Li*[,†]

[†]Center for Nanophase Materials Sciences, Oak Ridge National Laboratory, Oak Ridge, Tennessee 37831, United States

[‡]Department of Physics and Astronomy, University of California, Irvine, California 92697, United States

[§]Department of Physics and Astronomy, The University of Tennessee, Knoxville, Tennessee 37996, United States

[∥]Department of Physics, The University of Texas at Austin, Austin, Texas 78712, United States

Supporting Information

ABSTRACT: Quantum wires, as a smallest electronic conductor, are expected to be a fundamental component in all quantum architectures. The electronic conductance in quantum wires, however, is often dictated by structural instabilities and electron localization at the atomic scale. Here we report on the evolutions of electronic transport as a function of temperature and interwire coupling as the quantum wires of $GdSi_2$ are self-assembled on Si(100) wire-by-wire. The correlation between structure, electronic properties, and electronic transport are examined by combining nanotransport measurements, scanning tunneling microscopy, and density functional theory calculations. A metal−insulator transition is revealed in isolated nanowires, while a robust metallic state is obtained in wire bundles at low temperature. The atomic defects lead to electron localizations in isolated nanowire, and interwire coupling stabilizes the structure and promotes the metallic states in wire bundles. This illustrates how the conductance nature of a one-dimensional system can be dramatically modified by the environmental change on the atomic scale.

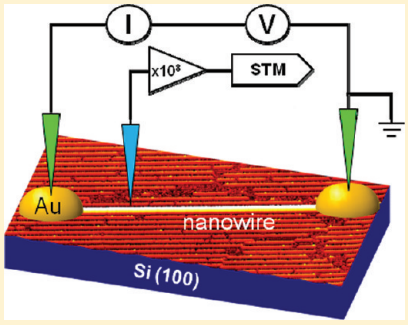

KEYWORDS: *Electronic transport, nanowire, defects, electronic coupling, localization, electronic density of states, scanning tunneling microscopy*

Quantum wires are extremely narrow one-dimensional (1D) materials where electron motion is allowed only along the wire direction but confined in the other two directions.[1,2] Quantum wires often exhibit electronic transport properties qualitatively different from their counterparts in higher dimensions.[3,4] It was realized in 1950 by Tomonaga[5] that due to the enhanced electron−electron interaction in a 1D system, the Fermi liquid description of electrons is no longer valid; instead, a 1D system needs to be described by collective excitations now known as a Luttinger liquid.[6] However, the Luttinger liquid theory is strictly limited to low-energy excitations with linear electron dispersions.[7] In real materials, 1D systems are inevitably coupled to their environment, where the interactions with substrates, defects, and neighboring nanowires may alter the electronic structure, rendering a nonlinear electron dispersion and even opening a band gap. Atomic scale defects can drive a 1D electron system to an insulating state when the electron wave functions become localized in valleys of the potential landscape.[3,8,9] Interwire coupling was suggested by Abrikosov et al.[10] to suppress the localization effect, but Prigodin et al.[11] argued that all states in a 1D system should be localized even in the weak localization case. The information on local structure and electronic properties is thus pivotal to the understanding of 1D transport.

Experimentally, the local electronic structures of quasi-1D systems are commonly probed by using scanning tunneling microscopy (STM) and angular resolved photoemission spectroscopy (ARPES). A finite density of states (DOS) near the Fermi level, suggestive of metallic characteristics, has been revealed in a wide range of 1D systems from single-wall carbon nanotubes[12] to quasi-1D surface reconstructions induced by Au or In on Si surfaces.[13,14] However, the local DOS exhibits a spontaneous metal−insulator transition (MIT) at low temperature due to a symmetry-lowering lattice deformation or charge density reorganization in most 1D systems.[9,13−15] Silicide nanowires self-assembled by depositing Dy, Ho, Er, Gd, Sm, and Y on the Si (100) substrate[16−18] are another prototype of 1D systems and are of great interest as interconnects in nanoelectronic devices. A metallic band structure has been revealed in $GdSi_2$ nanowires,[18] while a fluctuating charge order has also been reported in YSi_2 nanowires at low temperatures.[19] In spite of several attempts at macro- to mesoscopic length scale,[20−22] a direct correlation between electronic transport and local electronic and structural properties down to the atomic

Received: November 14, 2011
Revised: January 18, 2012
Published: January 23, 2012

scale remains an open question for these quantum wires, which hinders their application in novel devices.

Here we try to examine the intrinsic transport−structure relations down to the atomic scale by growing $GdSi_2$ quantum wire systems wire-by-wire and performing both STM and nanotransport measurements on the same system, as schematically illustrated in Figure 1a. In particular, we examine the effects of atomic defects and interwire coupling on the transport properties of self-assembled nanowires.

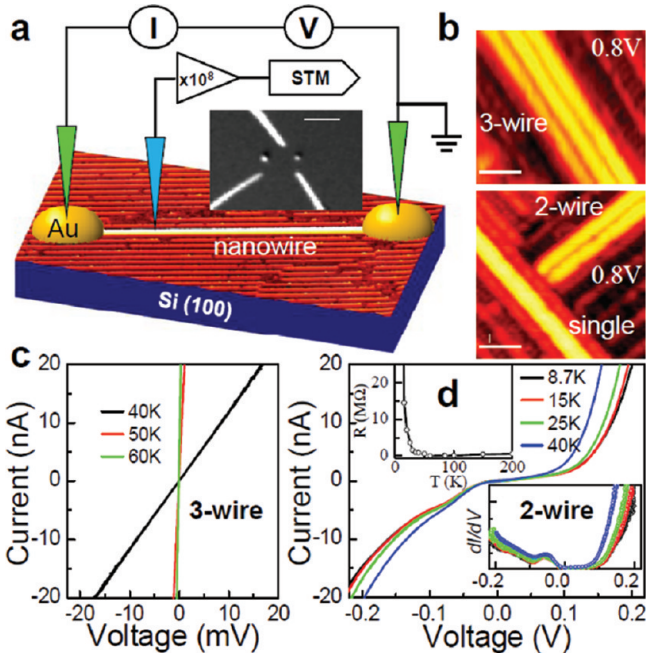

Figure 1. Electrical conductance of individual $GdSi_2$ nanowires from nanotransport measurements. (a) Schematic illustration of the measurement configurations for in situ electrical transport and local density of states on a single nanowire. Inset: SEM image of local Au contacts and Au-coated STM tip above a $GdSi_2$ nanowire. Scale bar: 1 μm. (b) STM images of single and double wires and a three-wire bundle. Scale bars: 4 nm. (c) Transport $I(V)$ curves for a three-wire bundle. (d) Transport $I(V)$ curves for a double wire. Inset of lower panel: numerical transport dI/dV of the double wire. Inset of upper panel: Temperature-dependent resistance of the double wire.

$GdSi_2$ nanowires were grown on the Si(100) 2 × 1 surface by depositing Gd at 600 °C with a rate of 0.1−0.2 ML/min. The growth of $GdSi_2$ initially produces a Si(100)-Gd 2 × 7 surface reconstruction, which then serves as the template for the growth of well-ordered and uniformly oriented arrays of $GdSi_2$ nanowires.[23] Both "isolated" nanowires and bundles of two or more $GdSi_2$ nanowires with atomic spacing can be obtained by controlling the Gd coverage and growth parameters. The anisotropic growth can be rationalized by considering the anisotropic lattice mismatches along the two orthogonal crystallographic directions of $GdSi_2$ and Si: the lattice mismatch in the $[0001]_{GdSi2}/[1\bar{1}0]_{Si}$ direction is +8.6%, whereas it is only +0.8% in the $[11\bar{2}0]_{GdSi2}/[110]_{Si}$ direction, so that nanowire grows preferably along the $[110]_{Si}$ direction. The representative STM images of single nanowire and two- or three-wire bundles are shown in Figure 1b.

The electron transport of nanowires was measured in situ with a four-probe STM system.[24] The width of the $GdSi_2$ nanowires is much smaller than that of the STM tip apex, and hence special local contacts are needed to bridge nanowires to STM probes for transport measurements. To fabricate nanocontacts in ultra high vacuum, a gold-coated tungsten tip was first located on top of the nanowire in a STM scanning mode. The tip was then slowly lowered toward the nanowire surface with a 15 V bias applied between the sample and the tip (tip negative). As soon as the tunneling current jumped to ~100 nA, which usually happens at a threshold field of ~3.5 V/Å, Au was deposited (50−200 nm in diameter) from the tip onto the surface via a field-induced atomic emission process.[25] Finally, the deposited Au nanoislands were contacted by two new STM tips with Au-coatings using a scanning electron microscope (SEM) integrated in the four-probe STM system, as shown in the inset of Figure 1a. This allows for in situ transport measurements on a particular nanowire addressed by STM.

We first examine the transport characteristics of $GdSi_2$ nanowires. At room temperature, both single wires and wire bundles exhibit linear $I(V)$ characteristics in transport measurements, indicative of a metallic conductance and the ohmic nature of the Au/$GdSi_2$ contacts. At lower temperatures, below 50 K, the linear $I(V)$ behavior and the metallic conductance only persist for nanowire bundles that consist of three or more nanowires, as shown in Figure 1c for a three-wire bundle. In contrast, $I(V)$ curves of single and double nanowires become nonlinear at low temperatures. As an example, the numerical dI/dV curves of a double wire in Figure 1d display a clear conductance gap of ~95 mV, indicating an insulating state at low temperature. A metal−insulator transition is confirmed by measurements of nanowire resistance (R) as a function of temperature (T), which reveal a MIT in a double wire at about 50 K (shown in the upper inset in Figure 1d). Furthermore, the transport $I(V)$ curves (Figure 1d) lose symmetry about $V = 0$ at low temperatures, which suggests the asymmetric coupling between two electrodes to the nanowire. The dI/dV curves display a resonance-like peak at about −55 mV, shown in the inset in Figure 1d, which is believed to come from a resonant tunneling process of electrons between one electrode and the defect state in the nanowire as discussed later. To rule out the possible contribution of substrate conductance, we also measured the transport $I(V)$ curves of the (2 × 7) reconstructed Gd/Si(001) surface without a nanowire. The surface layer is insulating with resistance orders of magnitude higher than that of the nanowires. Consequently, the substrate conductance is negligible and does not affect our measurements of the wire transport.

We then characterize the local structures of $GdSi_2$ nanowires with STM. Figure 2a shows two "isolated" nanowires that each has an apparent width of 16.7 Å, a height of 4 Å, and lengths up to several micrometers. Interestingly, dual bias images (Figure 2b) and height profiles (Figure 2c) of the single wire show bright protrusions (0.5−0.9 Å) along the nanowire. The filled and empty states of protrusions appear to be in phase, in contrast with YSi_2 nanowires where the protrusions are out-of-phase and associated with charge ordering along the nanowire.[19] The statistical distributions of separations between neighboring protrusions strongly favor odd multiples of the Si surface lattice constant ($a_{Si} = a_0/\sqrt{2} = 3.84$ Å, where a_0 is the lattice constant of the bulk Si). As shown in Figure 2d, more than 94% of them are separated by distances of 3, 5, 7, and 9 a_{Si}. In addition, a smaller corrugation with × $2a_{Si}$ periodicity appears along the nanowires as marked with dashed circles in Figure 2b.

dx.doi.org/10.1021/nl204003s | Nano Lett. 2012, 12, 938−942

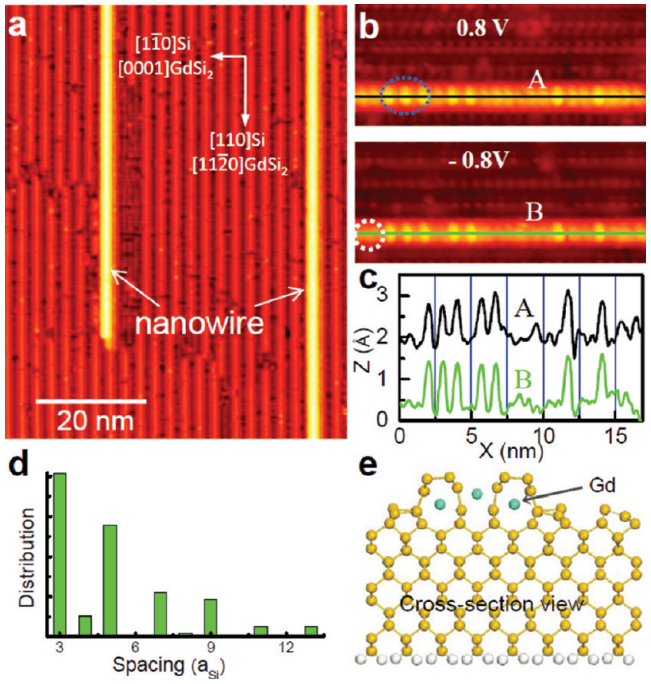

Figure 2. Structure of single nanowire from STM and DFT. (a) STM image showing well-ordered and uniformly oriented $GdSi_2$ single nanowires. (b) Zoom-in STM images of $GdSi_2$ single nanowire at dual sample bias of +0.8 and −0.8 V, respectively. Dashed circle and oval mark the regions with × $2a_{Si}$ and × $3a_{Si}$ corrugations, respectively. (c) Line profiles along the nanowire at dual sample bias. Profile curve A is shifted up by 1.5 Å for clarity. (d) Statistical distributions of the spacings between neighboring bright protrusions at 80 K. (e) Cross-sectional view of the calculated structure of a single $GdSi_2$ nanowire.

Structures based on STM images are refined through ab initio calculations using the density functional theory (DFT). DFT calculations were performed by using the Vienna ab initio simulation package (VASP) at the level of the generalized gradient approximation (GGA). We employed a slab model, using 12 atom-layer Si and $GdSi_2$ along with a vacuum region of 15 Å. The dangling bonds at the bottom surface were passivated by a monolayer of hydrogen atoms. To mimic the environment of a single nanowire, supercells as large as (3 × 10) were tested in the lateral plane and (n × 8) supercells were found to be sufficiently large to study two isolated wires. The validity of VASP for the treatment of Gd was established in the literature[26] and also tested in our own calculations. The spin−orbit coupling is not considered in this case since the Gd-4f is full in the majority spin channel and empty in the minority spin channel.

The optimized structure of a $GdSi_2$ single wire with a (1 × 8) supercell ($1a_{Si}$ along the wire and $8a_{Si}$ across) consists of two parallel Si dimer rows, where the Gd atoms are located underneath dimers and in the troughs between the dimer rows, similar to that reported for YSi_2 nanowires.[19,27] The main difference between Y and Gd is that Gd is magnetic and also induces spin polarization on the Si atoms, with a local magnetic moment of 7.3 μ_B per Gd atom aligning ferromagnetically (↑↑↑) across the single wire in its ground state. Further structural optimization with larger supercells (Figure S1, Supporting Information) shows noticeable reconstructions at the base along the wire, with energy gains of 62 meV/a_{Si} for a (2 × 8) unit cell and 72 meV/a_{Si} for a (3 × 8) unit cell, respectively. Si adatoms can be stabilized on the nanowire especially on the (3 × 8) reconstructed one (Figure S1, Supporting Information), taking sites between two central Gd atoms along the axis of nanowire, corroborating the STM observations in Figure 2b. Thus, the bright protrusions in Figure 2b are believed to correspond to Si adatoms as seen in atomic chains of Si(111)-Au.[28]

The structures of bundle wires are shown in Figure 3 for a seven-wire bundle. The nanowire bundle has × $5a_{Si}$ (1.92 nm)

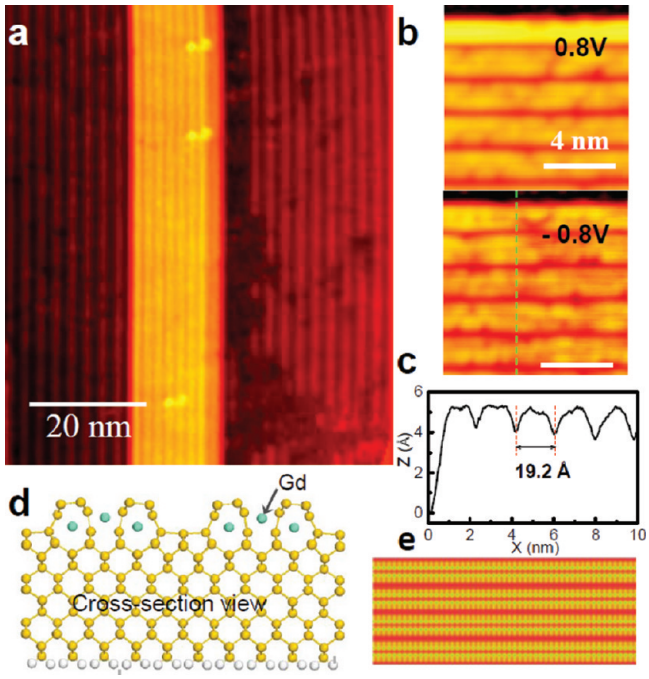

Figure 3. Structure of nanowire bundle from STM and DFT. (a) STM image showing a seven-wire bundle. (b) Zoom-in STM images at dual sample bias of +0.8 and −0.8 V, respectively. (c) Line profile across the $GdSi_2$ nanowire bundle showing a × $5a_{Si}$ periodicity. (d) Cross-sectional view of the calculated structure of the $GdSi_2$ nanowire bundles. (e) Simulated STM image of $GdSi_2$ nanowire bundles at −1.5 V in a constant current mode.

period across its width, with ∼2.5 Å ($5a_{Si}$-16.7 Å) interwire spacing, as shown in the image and line profile in Figure 3b,c. Interestingly, the adatom defects, which are so prominent on the isolated nanowires in a wide bias range, appear only sparsely at 1.5 V on the bundle wires (Figures S3−S5, Supporting Information). Moreover, adatoms are not seen on double wires and on the edges of the bundle wires. The density statistics show that the averaged spacing between adatoms on bundle wires (excluding edge wires) is 3.2 nm, much larger than the spacing of 1.8 nm on single wires. The optimized structural model and simulated STM image from the DFT calculations are shown in Figure 3d,e. The details of DFT calculations are presented in Supporting Information. Similar to experimental finding, DFT calculations suggest that the presence of Si absorption or reconstructions along the base is much less preferred in wire bundles in comparison with the single wires (Figure S2, Supporting Information). The distance between the two outer Gd rows shrinks slightly to 8.00 Å in bundles from 8.08 Å in a single wire, but the base of nanowire is noticeably (0.4 Å) wider in bundles than in a single wire. Evidently, interwire coupling enhances the structural stability of the bundle wires. In addition, the magnetic ordering changes to ferrimagnetic (i.e., ↑↑↓) with a local moment of 7.1 μ_B for each

dx.doi.org/10.1021/nl204003s | Nano Lett. 2012, 12, 938−942

Gd atom. Note, in a double wire, the width of two wires is the same as that of a single wire, with an interwire spacing of 16.9 Å, noticeably smaller than the wire spacing (19.2 Å) in a bundle wire, as shown in Figure S6, Supporting Information. Thus, the structure of double wire appears more like a single wire than a bundle wire.

We now examine the correlation between electronic transport and local density of states of $GdSi_2$ nanowires. STS measurements on single, double, and bundle nanowires at 80 and 6 K are shown in Figure 4a,b, respectively. At 80 K, single, double, and bundle nanowires all show finite DOS near the Fermi level (E_F), confirming their metallic nature. At 6 K, the DOS of single and double wires both show a small gap at 6 K, with more evident DOE suppressions for the single wire. The DOS of a bundle wire remains finite near E_F at 6 K, confirming the previous ARPES reports for the bundle wires.[18] At both temperatures, the DOS in the middle of the bundle wire is significantly higher than that at the edge. To better understand the origin of the MIT for a single nanowire, we map the spatial distributions of STS along the single nanowire in the inset of Figure 4b, which shows strongly fluctuating pseudoband gap, particularly in the defect regions, as highlighted by the blue color and white vertical dash lines in the inset of Figure 4b. The pseudogap is wider near defects. The main features of the normalized STS, $(dI/dV)/(I/V)$, spectra are overall reproduced by the calculated DOS projected to a region 3 Å above the wire, as shown in Figure 4c for the bundle wire and in the inset for the single wire, respectively. The evolution from nonconducting single and double nanowires, and relatively conducting wire bundle at the edge, to the robust metallic state in the middle of a wire bundle is well correlated with the presence of interwire coupling.

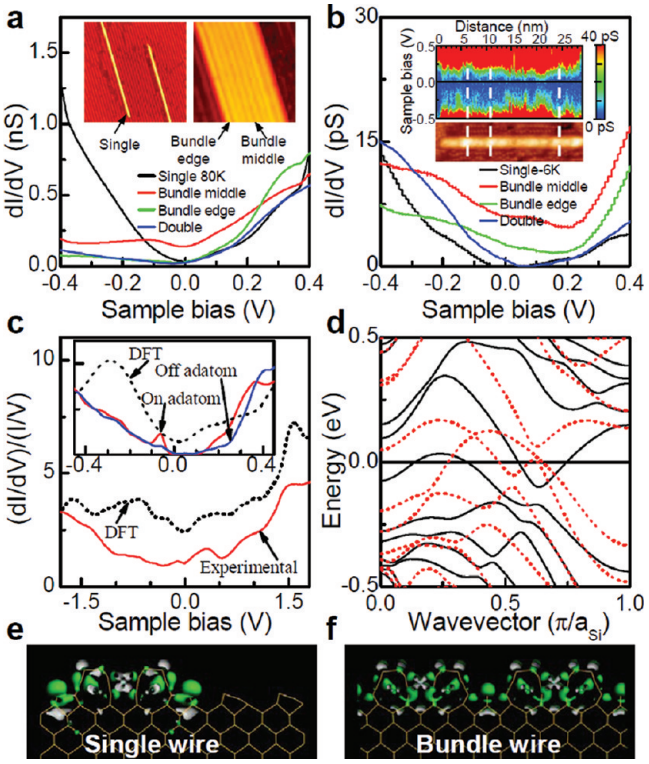

Figure 4. Electronic structure of single and double wires and wire bundle from STS and DFT. (a) dI/dV spectra at 80 K on $GdSi_2$ single wire (black), double wire (blue), bundle center (red), and bundle edge (green). Inset: STM images of the single and bundle wires. (b) dI/dV spectra at 6 K on $GdSi_2$ single wire (black), double wire (blue), bundle center (red), and bundle edge (green). Insets: the spatial variations of dI/dV spectra as a function of energy along a single wire. White dashed lines mark the locations of adatoms. (c) Comparison of the measured $(dI/dV)/(I/V)$ spectrum at 10 K and the calculated DOS projected to a region 3 Å above the bundle wire. Inset: $(dI/dV)/(I/V)$ spectra of a single wire measured at 10 K on an adatom and 2 nm away from the adatom defect, and the calculated DOS without adatoms. (d) Calculated band diagram of $GdSi_2$ single wire along the wire ($\Gamma-X$) for majority (solid black) and minority spins (dashed red). (e) Cross-sectional view of the calculated wave function distributions for states around the Fermi level of single and (f) for bundle wires. Green and gray represent outer and inner sides of the isosurfaces.

The transport properties of single nanowires are dictated by the atomic defects. Figure 4d shows the calculated band structures of a single unreconstructed $GdSi_2$ nanowire, exhibiting a metallic feature with several bands crossing E_F in both the majority (solid lines) and minority (dashed lines) spin channels. The presence of atomic defects leads to a pseudogap, as demonstrated in the inset of Figure 4b. Adatoms that are stable on the single wires can act as pinning centers, destroying the long-range order of the electronic potential[29] and hindering the electron transport. The impurity effect in a 1D chain has been simulated by Fogler et al.,[29] who found that the impurities can divide the chain into metallic segments. Addition or removal of electrons from such segments during the transport causes charge excitations with a Coulomb gap that increases with the impurity density. Massey and Lee have reported the first direct spectroscopic measurement of Coulomb correlation gap in a localized insulator Si:B system.[30] Although the gap values are of the order of 1 meV in the Si:B system, they should be significantly higher in 1D, as shown by Maji et al.[31] This picture agrees with our observations for single nanowires. In addtion, adatoms can create a defect-assisted tunneling channel, responsible for the resonance-like peak in the dI/dV curves in Figure 1d. When the energy level of adatoms aligns with E_F under bias, resonant tunneling occurs, and a surge in current can be observed, in analogous to the resonant tunneling in a semiconductor molecule−metal junction.[32] Indeed, the tunneling dI/dV curve taken on the defect site shows a small blip around −55 meV, and this feature disappears 2 nm away from the defect, as shown in the inset of Figure 4c. The asymmetry in the $I(V)$ curves in Figure 1d is thus due to the nonuniform distribution of atomic defects that opens resonant tunneling channel only near one electrode.

Interwire coupling helps to preserve the metallic state in bundle wires. With only $1a_{Si}$ spacing, adjacent nanowires inevitably interact with each other. Significantly, the × 2 and × 3 superstructures disappear in wire bundles and Si adsorptions become unstable; both effects making the metallic state more stable in bundles in contrast to the single wire cases. The interwire electronic coupling in bundle wires is further attested by the continuity of wave function of states within ±0.2 eV in between the constituent wires as shown in Figure 4e,f. By fitting the DFT bands to a tight-binding Hamiltonian, one may also get the interwire hopping integrals for different states, t_{inter}, and the largest value of t_{inter} is 0.09 eV per a_{Si}. The electronic behavior of a double wire (two-wire bundle) is relatively more similar to a single wire than a bundle wire since they both show a metal−insulator transition at low temperature. The insulating state in a single wire is localization induced, but the nature of gap opening in a double wire remains unclear here. Apparently, the interwire coupling in a double wire is overwhelmed by the

dx.doi.org/10.1021/nl204003s | Nano Lett. 2012, 12, 938−942

edge states, and metallic states are only stable when three or more wires are coupled.

In summary, we have examined transport and structure relations in a quantum wire system by performing both nanotransport and scanning tunneling microscopy measurements as the system is assembled wire-by-wire. The self-assembled $GdSi_2$ wires are grown in the form of either isolated single nanowires with atomic defects or bundles of nanowires with atomic interwire spacing. A field-induced atom emission process is utilized to fabricate local contacts as a bridge between the nanoscopic wires and the mesoscopic transport electrodes. The unique characterization approach has enabled us to examine the effects of atomic defects and interwire coupling on the electronic transport in a quantum wire system in situ in ultrahigh vacuum. A robust metallic conductance is revealed in a wire bundle with three or more constituent nanowires, stabilized by interwire coupling. In contrast, the isolated single nanowires exhibit a metal−insulator transition upon cooling due to localization effect. First-principles calculations reproduce the topographic structures and measured density of states and explain the nature of the electronic interactions between nanowires. The results provide a rare glimpse of the intrinsic structure−transport relations and the influence of local environments at an unprecedented atomic scale.

■ ASSOCIATED CONTENT

Supporting Information

Details on theoretical calculations of adsorption geometry and additional STM images on single nanowires and wire bundles. This material is available free of charge via the Internet at http://pubs.acs.org.

■ AUTHOR INFORMATION

Corresponding Author

*E-mail: apli@ornl.gov.

Notes

The authors declare no competing financial interest.

■ ACKNOWLEDGMENTS

This research was conducted at the Center for Nanophase Materials Sciences, which is sponsored at Oak Ridge National Laboratory by the Office of Basic Energy Sciences, U.S. Department of Energy. Work at UCI was supported by DOE grant DE-FG02-05ER46237. Calculations were performed on parallel computers at NERSC.

■ REFERENCES

(1) Barth, J. V.; Costantini, G.; Kern, K. *Nature* **2005**, *437*, 671−679.
(2) Wu, Y.; Xiang, J.; Yang, C.; Lu, W.; Lieber, C. M. *Nature* **2004**, *430* (6995), 61−65.
(3) Mott, N. F.; Twose, W. D. *Adv. Phys.* **1961**, *10* (38), 107−163.
(4) Peierls, R. E. *Quantum Theory of Solids*; Nature Publishing Group: New York, 1955.
(5) Tomonaga, S.-i. *Prog. Theor. Phys.* **1950**, *5*, 4.
(6) Luttinger, J. M. *J. Math. Phys.* **1963**, *4* (9), 1154−1162.
(7) Barak, G.; Steinberg, H.; Pfeiffer, L. N.; West, K. W.; Glazman, L.; von Oppen, F.; Yacoby, A. *Nat. Phys.* **2010**, *6* (7), 489−493.
(8) Anderson, P. W. *Phys. Rev.* **1958**, *109* (5), 1492.
(9) Snijders, P. C.; Weitering, H. H. *Rev. Mod. Phys.* **2010**, *82* (1), 307−329.
(10) Abrikosov, A. A.; Ryzhkin, I. A. *Adv. Phys.* **1978**, *27* (2), 147−230.
(11) Prigodin, V. N.; Firsov, Y. A. *JETP Lett.* **1983**, *38*, 5.
(12) Charlier, J. C.; Blase, X.; Roche, S. *Rev. Mod. Phys.* **2007**, *79*, 677−732.
(13) Lee, G.; Guo, J.; Plummer, E. W. *Phys. Rev. Lett.* **2005**, *95* (11), 116103.
(14) Yeom, H. W.; Takeda, S.; Rotenberg, E.; Matsuda, I.; Horikoshi, K.; Schaefer, J.; Lee, C. M.; Kevan, S. D.; Ohta, T.; Nagao, T.; Hasegawa, S. *Phys. Rev. Lett.* **1999**, *82* (24), 4898.
(15) Crain, J. N.; Kirakosian, A.; Altmann, K. N.; Bromberger, C.; Erwin, S. C.; McChesney, J. L.; Lin, J. L.; Himpsel, F. J. *Phys. Rev. Lett.* **2003**, *90* (17), 176805.
(16) Chen, Y.; Ohlberg, D. A. A.; Williams, R. S. *J. Appl. Phys.* **2002**, *91*, 3213−3218.
(17) Ohbuchi, C.; Nogami, J. *Phys. Rev. B* **2002**, *66* (16), 165323.
(18) Yeom, H. W.; Kim, Y. K.; Lee, E. Y.; Ryang, K. D.; Kang, P. G. *Phys. Rev. Lett.* **2005**, *95* (20), 205504.
(19) Zeng, C.; Kent, P. R. C.; Kim, T.-H.; Li, A.-P.; Weitering, H. H. *Nat. Mater.* **2008**, *7* (7), 539−542.
(20) Morikawa, H.; Kim, K. S.; Kitaoka, Y.; Hirahara, T.; Hasegawa, S.; Yeom, H. W. *Phys. Rev. B* **2010**, *82* (4), 045423.
(21) Tegenkamp, C.; Kallassy, Z.; Pfnur, H.; Gunter, H. L.; Zielasek, V.; Henzler, M. *Phys. Rev. Lett.* **2005**, *95* (17), 176804.
(22) Tegenkamp, C.; Lukermann, D.; Akbari, S.; Czubanowski, M.; Schuster, A.; Pfnur, H. *Phys. Rev. B* **2010**, *82* (20), 205413.
(23) Harrison, B. C.; Ryan, P.; Boland, J. J. *Surf. Sci.* **2005**, *582* (1−3), 79−89.
(24) Kim, T.-H.; Wang, Z.; Wendelken, J., F.; Weitering, H., H.; Li, W.; Li, A.-P. *Rev. Sci. Instrum.* **2007**, *78* (12), 123701.
(25) Mamin, H. J.; Guethner, P. H.; Rugar, D. *Phys. Rev. Lett.* **1990**, *65* (19), 2418.
(26) Petersen, M.; Hafner, J.; Marsman, M. *J. Phys.: Condens. Matter* **2006**, *18* (30), 7021−7043.
(27) Shinde, A.; Wu, R. Q.; Ragan, R. *Surf. Sci.* **2010**, *604* (17−18), 1481−1486.
(28) Yoon, H. S.; Park, S. J.; Lee, J. E.; Whang, C. N.; Lyo, I. W. *Phys. Rev. Lett.* **2004**, *92* (9), 096801.
(29) Fogler, M. M.; Teber, S.; Shklovskii, B. I. *Phys. Rev. B* **2004**, *69* (3), 035413.
(30) Massey, J. G.; Lee, M. *Phys. Rev. Lett.* **1995**, *75* (23), 4266−4269.
(31) Maji, S.; Mukhopadhyay, S.; Gangopadhyay, R.; De, A. *Phys. Rev. B* **2007**, *75* (7), 073202.
(32) Guisinger, N. P.; Yoder, N. L.; Hersam, M. C. *Proc. Natl. Acad. Sci. U.S.A.* **2005**, *102* (25), 8838−8843.